EFDA–JET–PR(10)35

E. Havlíčková, W. Fundamenski, V. Naulin, A.H. Nielsen, R. Zagórski,
J. Seidl, J. Horáček and JET EFDA contributors

Steady-State and Time-Dependent Modelling of Parallel Transport in the Scrape-Off Layer

Steady-State and Time-Dependent Modelling of Parallel Transport in the Scrape-Off Layer

E. Havlíčková[1], W. Fundamenski[1], V. Naulin[2], A.H. Nielsen[2], R. Zagórski[3], J. Seidl[4], J. Horáček[4] and JET EFDA contributors*

JET-EFDA, Culham Science Centre, OX14 3DB, Abingdon, UK

[1]EURATOM-CCFE Fusion Association, Culham Science Centre, OX14 3DB, Abingdon, OXON, UK
[2]Association EURATOM/Risø, National Laboratory for Sustainable Energy, OPL-128, P.O. Box 49, DK-4000 Roskilde, Denmark
[3]Association EURATOM/IPPLM, Institute of Plasma Physics and Laser Microfusion, Warsaw, Poland.
[4]Association EURATOM/IPP.CR, Institute of Plasma Physics, Prague, Czech Republic
** See annex of F. Romanelli et al, "Overview of JET Results", (23rd IAEA Fusion Energy Conference, Daejon, Republic of Korea (2010)).*

Preprint of Paper to be submitted for publication in
Plasma Physics and Controlled Fusion

ABSTRACT.
The one-dimensional fluid code SOLF1D has been used for modelling of plasma transport in the Scrape-Off Layer (SOL) along magnetic field lines, both in steady state and under transient conditions that arise due to plasma turbulence. The presented work summarizes results of SOLF1D with attention given to transient parallel transport which reveals two distinct time scales due to the transport mechanisms of convection and diffusion. Time-dependent modelling combined with the effect of ballooning shows propagation of particles along the magnetic field line with Mach number up to $M \approx 1$ and supersonic transport when plasma-neutral interactions are not present. Asymmetric heat and particle fluxes are analyzed for a case with poloidally asymmetric radial outflow (ballooning) and for a radial outflow with parallel momentum (rotation). In addition, parallel damping of the density and electron temperature calculated in SOLF1D is compared with the approximative model used in the turbulence code ESEL both for steady-state and turbulent SOL. Dynamics of the parallel transport are investigated for a simple transient event simulating the propagation of particles and energy to the targets from a blob passing across the flux tube at the outboard midplane and for time-dependent data provided by ESEL.

1. INTRODUCTION

The anomalous radial transport in the tokamak edge region is accepted to be caused by plasma turbulence. Experimental investigations and modelling of the turbulence and intermittent structures known as plasma blobs have been established with a certain success in describing these phenomena and revealing their driving mechanisms [2, 3, 4]. A number of codes has been developed to study the plasma turbulence in the edge/SOL region [5].

The ESEL code [6, 7] simulates electrostatic interchange turbulence in twodimensional geometry at the outboard midplane of a tokamak, perpendicular to the magnetic field. The computational domain involves the edge region with closed magnetic field lines, and the SOL and wall regions where magnetic field lines intercept divertor targets or the wall. Plasma and energy losses along the magnetic field to the targets in the open-field region are described by loss terms assuming subsonic advection of particles and classical Spitzer-H¨arm diffusion for energy transport (see section 3.1). Values of parallel loss terms are calculated from the local density and temperature as if we had a steady-state solution in the parallel direction, neglecting any effects of dynamics. It is expected, however, and also indicated by the presented investigations, that the parallel dynamics reveal rather a complex behaviour and it is desirable to describe the parallel transport in ESEL simulations in time-dependent way consistently with turbulent radial transport. It is therefore planned to improve ESEL parallel physics or couple ESEL with the SOLF1D code into a quasi three-dimensional model.

SOLF1D is a one-dimensional fluid code for modelling plasma transport in the SOL along magnetic field lines, the dimension missing in ESEL. SOLF1D solves a set of Braginskii-like equations [8] for electrons and ions and assumes ambipolarity and no net current. Plasma-neutral collisions are taken into account and neutrals are treated as a separate fluid. Cross-field transport

constitutes a source of mass and energy for the one-dimensional computational region and following the standard approach in the fluid modelling of the SOL, SOLF1D requires these cross-field sources on the input. Beside steady-state sources used to achieve a stationary solution, it is possible to solve time-dependent problems and use e.g. fluctuating sources which result from the edge turbulence in ESEL.

ESEL has been applied to TCV and JET discharges so far [7, 9] and these ESEL runs are of interest in this paper. Operational parameters are listed in [9]. It has been found, specifically for the low-collision L-mode plasma of a JET experiment, that the experimental radial profile of the temperature at the outboard midplane is reproduced well by ESEL simulation, while the density profile is not found to match the experiment. Simulation results indicate that a more precise treatment of parallel flows in ESEL is required and the description of the parallel transport is considered as the main weakness of ESEL. The ESEL model of parallel losses was derived for steady-state and simple SOL conditions. In low-collisionality regimes (the so-called simple SOL), we typically do not observe strong gradients of plasma parameters along the magnetic field and crossParallel transport in the SOL 3 field transport is the dominant source of SOL plasma. To satisfy the low-collisionality conditions, a kinetic correction known as the heat flux limiter [10, 11] is introduced. However, in the investigated case of the divertor TCV tokamak, we expect to find the SOL in a conduction-limited or detached regime when we observe a strong recycling of neutrals at the targets and the simple SOL assumption can be violated.

The following section (section 2) introduces the SOLF1D code. The first part of the paper (section 3) compares the simple ESEL model with the fluid description of SOLF1D for a steady-state SOL. In the second part (section 4), we focus on the parallel transport in transient conditions. Before coupling the two codes, which will lead to a rather complex system, it is useful to study the response of SOLF1D to large fluctuations in the one-dimensional system only. First, we analyze in detail the transit of a single blob and then the application of SOLF1D to ESEL output follows. Several cases are investigated in sections 4.1–4.5 including asymmetric cases where we calculate heat and particle fluxes on the targets (note that kinetic effects are neglected in the fluid code).

2. SOLF1D CODE

The SOLF1D code is based on a one-dimensional fluid model solving classical Braginskii equations (e.g. as the model in [12]) for the ion density ni, the parallel ion velocity ui, the electron temperature T_e and the ion temperature T_i

$$\frac{\partial n_i}{\partial t_i} + \frac{\partial}{\partial x}(n_i u_i) = S_i^n \tag{1}$$

$$\frac{\partial}{\partial t}(m_i n_i u_i) + \frac{\partial}{\partial x}\left(m_i n_i u_i^2 - \eta_i \frac{\partial u_i}{\partial x}\right) = -\frac{\partial p_i}{\partial x} + e n_i E + R_i + m_i S_i^u, \tag{2}$$

$$\frac{\partial}{\partial t}\left(\frac{3}{2} n_e k T_e\right) + \frac{\partial}{\partial x}\left(\frac{5}{2} u_e n_e k T_e + q_e\right) = -e n_e u_e E + u_e R_e + Q_e + S_e^E, \tag{3}$$

$$\frac{\partial}{\partial t}\left(\frac{3}{2}n_i kT_i + \frac{1}{2}m_i n_i u_i^2\right) + \frac{\partial}{\partial x}\left(\frac{5}{2}u_i n_i kT_i + \frac{1}{2}m_i n_i u_i^3 + q_i - u_i \eta_i \frac{\partial u_i}{\partial x}\right) = en_i u_i E + u_i R_i + Q_i + S_i^E \tag{4}$$

and assuming charge neutrality ne = ni and ambipolarity $u_e = u_i$ (no net parallel current $j_{\|} = 0$) and the electron momentum equation reduced to the generalized Ohm's law $en_eE = -\partial p_e/\partial_x + R_e$ from which the ambipolar electric field can be evaluated. S_i^n , S_e^E, S_e^E and S_i^E are sources of the mass, momentum and energy and include collision terms (ionization, charge exchange, recombination and excitation) and external sources of particles and energy into the flux tube S^n_{EXT} and S^E_{EXT} which are here supposed to appear due to cross-field transport. R_e and R_i ($R_e = -R_i$) are the thermal and friction forces, E is the parallel electric field, p_i and p_e is the ion and electron static pressure, i is the ion viscosity, mi is the ion mass and $q_e = -\kappa_e \partial(kT_e)/\partial x$ and $q_i = -\kappa_e \partial(kT_i)/\partial x$ are the thermal heat fluxes. Q_e and Q_i ($Q_e = -Q_i$) is the heating due to electron-ion collisions.

To solve the particle and energy balance in a one-dimensional flux tube, we need to know, in the input of the code, the amount of particles and energy entering the domain (S^n_{EXT} and S^E_{EXT}) and the size of the domain (the connection length L_c). We use classical transport coefficients, heat flux limiters are not used in the work that follows. The ion viscosity η_i, the electron and ion thermal conductivities κ_e and κ_i and the ion heating Qi are calculated from formulas given in [13]

$$\eta_i = 0.96 n_i kT_i \tau_i, \tag{5}$$

$$\varkappa_e = 3.2\frac{n_e kT_e \tau_e}{m_e}, \varkappa_i = 3.9\frac{n_i kT_i \tau_i}{m_i}, \tag{6}$$

$$Q_i = \frac{3m_e}{m_i}\frac{n_i k}{\tau_e}(T_e - T_i). \tag{7}$$

Standard sheath boundary conditions are incorporated $u_i = c_s = \sqrt{k(T_e + T_i)/m_i}$, $Q_i = \delta_i kT_i n_i u_i$ and $Q_e = \delta_e kT_e n_e u_e$ using the energy transmission coefficients of the sheath $\delta_i = 3.5$ and $\delta_e = 5.0$.

SOLF1D couples the plasma model with a one-dimensional fluid model of neutrals. In the SOL, the neutrals are assumed to be in a local thermal equilibrium with the ions due to charge-exchange processes, therefore they are considered to have the temperature locally equal to the ion temperature $T_0 = T_i$ everywhere in the SOL. The continuity and momentum transfer equations

$$\frac{\partial n_0}{\partial t} + \frac{\partial}{\partial x}(n_0 u_0) = S_0^n, \tag{8}$$

$$\frac{\partial}{\partial t}(m_0 n_0 u_0) + \frac{\partial}{\partial x}\left(m_0 n_0 u_0^2\right) = -\frac{\partial p_0}{\partial x} + m_0 S_0^u \tag{9}$$

are solved for the density of neutrals n_0 and their parallel velocity u_0 and taking into account changes of the density and momentum S_0^n 0 and S_0^u caused by collisions with plasma. p_0 and m_0

are neutral pressure and mass. It is assumed that neutrals are all ionized within the SOL and there is no cross-field source or sink to/from the computational domain. A target pumping is represented by the boundary condition $\Gamma_0 = -R\Gamma_i$ using the recycling coefficient R = 0.975 and u_0 at the boundary is prescribed to the neutral thermal speed $\sqrt{kT_0/m_0}$ (neutrals leaving the wall are assumed to equilibrate fast with plasma ions due to the charge exchange.) The system of nonlinear equations is solved by an algorithm based on the finite difference method. The equations are discretized on a non-uniform staggered grid using traditional numerical schemes and solved by a mixed explicit/implicit time integration. We use an exponential grid with refined spacing in boundary regions where large gradients can occur in high-recycling or detached regimes and the number of grid points in the parallel direction in presented runs was 100. The convective terms of the fluid equations are converted to finite difference expressions by the second-order upwind scheme and the diffusive terms are discretized by the Crank-Nicholson scheme. The time stepping is based on the second-order splitting method (see e.g. [14]). Nonlinear terms are treated explicitly, while linear terms are updated to a new time level implicitly. Resulting systems of linear equations are solved by the Progonka and Matrix Progonka methods described in [15].

3. STEADY-STATE PARALLEL TRANSPORT

3.1. ESEL MODEL

Plasma transport along magnetic field lines to divertor targets can be characterized by parallel particle density and energy loss times n and E. The model of parallel losses in ESEL assumes a steady-state simple SOL and calculates the parallel loss times for particles and energy from values of the density and temperature at the outer midplane [9]. The parallel loss terms are described as losses caused by subsonic advection

$$\tau_n \approx \frac{L_\parallel}{Mc_s} \tag{10}$$

with the sound speed cs and Mach number M (in ESEL M ≈ 0.5 is considered as the average value along the SOL if we assume the simple SOL with approximately linear Mach number between targets) and the Spitzer-H¨arm diffusion

$$\tau_E \approx \frac{\frac{3}{2}L_\parallel^2 n_e}{\varkappa_e^{lim}} \tag{11}$$

with modified heat conductivity κ_e^{lim} using heat flux limits to satisfy all SOL collisionality regimes. The length scale of parallel density and temperature variations $L_\parallel$ (in general distinct for the density and temperature) is assumed equal to the connection length L_c. The following work is linked to the most documented ESEL results [7, 16], a simulation of interchange turbulence in the TCV tokamak with the separatrix density and electron temperature $n_{sep} \approx 2\times10^{19}$ m^{-3} and $T_{sep} \approx 20$eV. We use the connection length $L_c = 15$m (calculated from the LIUQE equilibrium reconstruction for typical TCV shot in the divertor configuration).

3.2. SOLF1D MODEL

The SOLF1D model was compared with the ESEL model in steady state as a first approach to estimate the possible impact of the fluid description on the strength of parallel damping for various collisionality regimes and to see if the approximations (10) and (11) remain valid under high-recycling conditions that are typically observed in divertor tokamaks and that were experimentally achieved in the investigated TCV case.

A parameter scan has been carried out changing values of the cross-field sources S^{n}_{EXT} and S^{E}_{EXT} and corresponding steady-state solutions were used to calculate parallel loss times. Uniform cross-field sources were considered along the SOL consistent with the assumption $L_{\|} = L_c$ of the ESEL model and the equations

$$\frac{\partial}{\partial x}(n_i u_i) \approx \frac{n_i}{\tau_n}, \tag{12}$$

$$\frac{\partial}{\partial x}\left(\frac{5}{2}u_e n_e k T_e + q_e\right) \approx \frac{\frac{3}{2}n_e k T_e}{\tau_E} \tag{13}$$

evaluated at the midplane (the upstream location in SOLF1D) were used as the definition for the parallel particle density and energy loss times, a more general from which the equations (10) and (11) can be derived under the simple SOL picture. The condition of quasi-neutrality $n_e = n_i$ is assumed. Note that the equations (12) and (13) do not take into account collision terms as their contribution to the parallel transport at the midplane is considered negligible.

3.3. COMPARISON

The parallel loss times are plotted as a function of the electron collisionality

$$\nu_e^{*} = \frac{L_c}{\nu_e^{th}\,\tau_e} \tag{14}$$

a parameter characterizing the operational regime of a tokamak defined as the ratio of the connection length L_c and the electron collision length. The electron collision time is taken to be

$$\tau_e = \frac{3\sqrt{m_e}(kT_e)^{3/2}}{4\sqrt{2\pi}n_e\lambda e^4} \tag{15}$$

as given in [13] and using the Coulomb logarithm $\lambda = 17$. The collisionality is calculated from the upstream values of the density and temperature. Note that τ_n and τ_E are not uniquely determined by the collisionality, from (10) and (11) we get τ_E/τ_n if we assume $L_{\|} = L_c$. However, a wider scan over both S^{n}_{EXT} and S^{E}_{EXT} shows the same trend. The results presented in Fig.1 compare SOLF1D (red) and ESEL (black) values for a scan over the particle source S^{n}_{EXT}, while keeping the energy input S^{E}_{EXT} constant. Fair agreement has been obtained for the parallel energy loss time τ_E in the investigated collisionality range and it appears that the simple model based on the heat diffusion is

a good approximation in a steady state. The power to the targets is carried mostly by the conduction (compare the yellow and red points in Fig.1), only at very weak collisionalities does the convection also play a role. A remarkable difference has been found in the comparison of the parallel density loss times τ_n in the whole collisionalityrange and equation (10) seems to be too approximate estimate even in the steady-state case.

In figure 1, the first run of SOLF1D corresponding to the lowest collisionality coincides precisely with the ESEL model. If we look at steady-state parallel profiles of plasma parameters for this run (Fig.2 top) and the run 4 (Fig.2 bottom), we can notice a transition from a recycling regime with typical higher plasma density at the targets and SOL balance influenced by the ionization of neutrals in the divertor region, to a simple SOL regime with characteristic flat profile of the temperature and a parabolic profile of the density.

With increasing collisionality, a high-recycling system is formed in front of the target and if we go even further, we approach a limit ($T_e \approx 5$eV) for transition to detachment. In SOLF1D, we observe an onset of such regime when the particle flux on the target starts to decrease (Fig.3) due to charge-exchange momentum losses, while the ionization becomes less important. The charge-exchange process starts to dominate, but the recombination is still weak for target temperatures above 2eV. It is worth mentioning that the code does not take into account the influence of impurities that sufficiently cool the plasma further, making the momentum removal more efficient. It could be also noted that the upstream density is usually the controlling parameter in monitoring a transition to the detached regime, while here, changing the particle source S^n_{EXT} with a constant step does not make a big change of the upstream density at higher collisionalities, since in such regimes, the cross-field particle source becomes less important source of plasma in the SOL compared to ionization within the SOL and the plasma in the SOL is mainly sustained due to high recycling. Figure 3 shows also a departure from the total pressure conservation. Here the total pressure ptot is calculated as a sum of static and dynamic components. Constant total pressure between targets would correspond to the two-point model [17, 18] assuming that parallel sources or sinks of momentum due to plasma-neutral collisions are not present and neglecting viscous effects.

In the complex SOL, steep gradients of the plasma density develop close to targets as a consequence of a strong source by the ionization of neutrals (the dominant source of the SOL plasma). This effects on parallel gradients in the SOL which drive plasma transport and determine also the parallel losses calculated at the midplane. The simulation without neutrals in Fig.4 (we would observe parabolic-like profiles of the density) shows that the simple expression (10) for τ_n is justified for the simple SOL and we can assume $L_{\|} = L_c$ (consistent with linear Mach number). On the other hand, the heat convection starts playing a role in the heat transport and the equation (11) becomes less accurate. Note that the scan in Fig. 4 is a rather artificial simulation of the simple SOL in sense that plasma-neutral interactions and neutral recycling are not present within the flux tube and the cross-field flux represents the only plasma source in the whole collisionality range.

The discrepancy between τ_n calculated in SOLF1D and by the model used in ESEL in the steady-

state case (Fig.1) has been explained by the assumption of the simple SOL in ESEL. Other relevant effects important for this analysis will be discussed in the following section. Here uniform cross-field sources were considered in the fluid model. The distribution of the sources S^n_{EXT} and S^E_{EXT} (we assume the same SEEXT to electron and ion channels) along the SOL will surely affect $L_{\|}$. In real experiments, radial flows from the main plasma to the SOL are predominantly concentrated around the outboard midplane due to poloidal asymmetries [19] and the parallel profiles of the sources should be better described e.g. by a Gaussian function localized at the midplane. Such peaked sources would shape the parallel profiles of plasma parameters and influence the length scales of parallel variations of the density and temperature $L^n_{\|}$ and $L^T_{\|}$ and the strength of particle and energy parallel losses. We can further expect that this ballooning effect plays a role in determining the parallel loss terms especially in a time-dependent case, when the flux tube is fueled at the outboard midplane by intermittent turbulent transport.

4. TRANSIENT PARALLEL TRANSPORT

Plasma turbulence in the edge/SOL regions of a tokamak is locally manifested as strong fluctuations of the density, temperature, potential and other plasma parameters (see e.g. ESEL output in Fig.5). Turbulent structures, which are seen as blobs at the outboard midplane, tend to form filaments along the magnetic field due to rapid parallel transport. Consistently, the ESEL model assumes $L_{\|} = L_c$. Two-dimensional multifluid edge/SOL transport codes such as SOLPS or EDGE2D [20]-[23] do not take into account these plasma fluctuations and are typically run in steady-state fashion using average values of physical quantities. In the following, time-dependent simulations are presented where we focus on the SOL plasma dynamics and investigate the way particles and energy of transient blobs passing across the flux tube are carried to the targets and how $L_{\|}$ changes in the transient case. The effect of plasma fluctuations on calculation of parallel transport parameters has been further investigated in [24].

4.1. SIMULATION FOR TCV PARAMETERS

4.1.1. Input data and initial steady state

The simulation in section 4.1 is a reference case of the paper. We again use parameters of the TCV tokamak with the connection length $L_c = 15$m and parallel profiles of cross-field sources of plasma and energy are prescribed as Gaussian functions localized at the midplane (symmetric situation is considered) with the poloidal angle approximately $\pm 30^{\mathrm{o}}$. This value was chosen according to experimental observations reported in [19]. ESEL provides fluctuations of the density and temperature in time at each point of the ESEL domain. Figure 5 shows the ESEL output at the selected radial position $\rho = 0.2$. The average plasma density and electron temperature at this position are $\langle n_i \rangle = 1.5\times10^{19}\,\mathrm{m}^{-3}$ and $\langle T_e \rangle = 12.8$eV. Corresponding cross-field sources S^n_{EXT} and S^E_{EXT} required as the input for SOLF1D were evaluated from the equations

$$\frac{\partial n_e}{\partial t} + S^n_{EXT} + S^n_{\parallel} = 0, \tag{16}$$

$$\frac{\partial}{\partial t}\left(\frac{3}{2} n_e k T_e\right) + S^E_{EXT} + S^E_{\parallel} = 0 \tag{17}$$

and parallel damping terms $S_{\parallel}^{n}$ and $S_{\parallel}^{E}$ were calculated according to the approximative model of parallel transport in ESEL, which makes a certain inconsistency with the SOLF1D code. The obtained values S^{n}_{EXT} and S^{n}_{EXT} are radial sources at the outboard midplane, the interface of the two codes, which is modelled as the central upstream location in SOLF1D.

Sources averaged over the whole investigated time interval were used for obtaining a steady-state solution (Fig.6) and profiles of plasma parameters in the steady state were used as the initial condition that is required at the beginning of the calculation. Figure 7 shows individual contributions of all calculated terms to the total parallel losses $S_{\parallel}^{n}$ and $S_{\parallel}^{T}$. In a steady state, the sum of these terms should balance exactly the corresponding cross-field sources S^{n}_{EXT} and S^{T}_{EXT}. We can see that collision terms are negligible at the midplane, particles are convected (green), while the conduction (blue) dominates the heat transport.

4.1.2. Transient burst and its dynamics

At first, only one transient event has been analyzed. The sources of particles and energy to the flux tube from a passing blob are simplified as a step (rectangular) function in time with a realistic duration and intensity according to the ESEL output. The transient burst appears at t = 0.03ms with the duration 1μs. In Figure 8, we can see parallel profiles of the plasma density, velocity and electron temperature at three selected moments: t = 0.025ms (the steady state), t = 0.031ms (the maximum density and temperature) and t = 0.075ms. The upstream density and temperature jump up rapidly as the sources localized at the midplane are raised and a response at the targets is observed later. It appears that the temperature tends to flatten out faster than the density (see the red curve) as the power is quickly transported to the targets by the heat diffusion. Particles propagate to the targets as two density peaks by convection (see the green curve) and we can notice that the plasma velocity increases compared to the steady-state value. Plasma flow is driven by local parallel gradients represented by a pressure peak arising from the transient perturbation, while in the initial steady state, plasma flow is nearly stagnant in the most of the SOL in such high-recycling regime as the investigated case, which was discussed in the previous section (Fig.2). The velocity of the perturbation transit along the SOL (calculated as the velocity at the actual position of the particle peak and normalized by the local ion sound speed) is shown in Fig. 8. We observe subsonic transport and slowing down close to the target due to plasma-neutral friction. A slow relaxation back to the steady-state solution follows.

Temporal characteristics of the parallel transport reveal two distinct time scales. Figure 9 shows the time evolution of the plasma density. Before particles of the burst hit the target (the main maximum

at t = 0.17ms corresponding to the convection temporal scale), a noticeable maximum of the density appears at the boundary after much shorter time interval. This increase of the density at t = 0.07ms is a consequence of stronger ionization of recycling neutrals due to the increasing temperature. This happens on the time scale that corresponds to the heat conduction. In Fig.9 on the right, an echo effect is visible as some plasma propagates back to the SOL from the boundary region. Two time scales can be also deduced from Fig.10 where we plot target parameters during the transient. Note that Fig.10 displays values precisely at the target (boundary conditions), while in Fig.9, the density maximum in the boundary region is in the ionization zone in front of the target.

4.1.3. Parallel losses and comparison with a simple model

A detailed view in Fig.11 shows the parallel density and energy losses and contributions of the conduction and convection to the power transport. The strength of parallel losses of particles and energy can be described by parallel loss times τ_n and τ_E or τ_T defined by the relations

$$S_{\parallel}^{n} \equiv \frac{n_e}{\tau_n}, \quad S_{\parallel}^{E} \equiv \frac{\frac{3}{2} n_e k T_e}{\tau_E}, \quad S_{\parallel}^{T} \equiv \frac{T_e}{\tau_T}. \tag{18}$$

The total parallel losses $S^{n}_{\parallel}$, $S^{E}_{\parallel}$ and $S^{T}_{\parallel}$ are calculated in the SOLFID code as

$$S_{\parallel}^{n} = \frac{\partial}{\partial x}(n_i u_i) + S_{coll}^{n}, \tag{19}$$

$$S_{\parallel}^{E} = \frac{\partial}{\partial x}\left(\frac{5}{2} u_e n_e k T_e + q_e\right) - u_e \frac{\partial p_e}{\partial x} - Q_e + S_{coll}^{E}, \tag{20}$$

$$S_{\parallel}^{T} = \frac{\partial}{\partial x}(u_e T_e) + \frac{2}{3 k n_e}\frac{\partial q_e}{\partial x} - \frac{T_e}{3}\frac{\partial u_e}{\partial x} + \frac{2 m_e}{m_i \tau_e}(T_e - T_i) + S_{coll}^{T} \tag{21}$$

and they take into account the collision terms S^{n}_{coll}, S^{E}_{coll} and S^{T}_{coll}. The resulting parallel particle density loss time τ_n and the electron cooling time τ_T are plotted in Fig.12 as functions of time. Their values are compared with the ESEL model defined by the equations (10) and (11). We can conclude that ESEL underestimates the parallel losses in the analyzed transient case. Further, Fig.12 shows the total parallel density and temperature losses $S^{n}_{\parallel}$ and $S^{T}_{\parallel}$ as functions of the density and temperature and we can see that the assumption of constant parallel loss times which was used in several ESEL runs (and which means that $S^{n}_{\parallel}$ scales linearly with the density and $S^{T}_{\parallel}$ is proportional to the temperature) is a crude approximation in the transient case. The behaviour is more complex and we can hardly parametrize $S^{n}_{\parallel}$ and $S^{T}_{\parallel}$ as functions of the local density and temperature. Note that $S^{n}_{\parallel}$ in Fig.12 goes anti-clockwise in time, while $S^{T}_{\parallel}$ goes clockwise, because $S^{T}_{\parallel}$ reaches the maximum before the maximum temperature (as the heat is instantly carried to the target by the fast diffusive process). From the illustrations above (Fig. 8, 9 and 11), we can conclude that the assumption $L_{\parallel} = L_c$ is more relevant for the temperature (heat diffusion time scale) than for the particle transport (convection time scale). This can help to explain why good agreement between the

ESEL simulation and experiment for the JET low-collision Ohmic plasma in [9] has been achieved for the temperature radial profile, while the length scale of density variations should be shorter to see a match with experiment for the density.

4.2. Simulation with broader cross-field source

It can be seen, that while in the steady-state scan in the previous section, parallel loss times calculated by the fluid code were longer than characteristic times calculated in ESEL, it is the other way round in Fig.12 at the initial steady state. This trend is caused by peaked parallel profiles of radial sources, taking into account the ballooning character of radial transport. To see the importance of source distribution in the parallel direction in the transient case, we present results (Fig.13) for a source in the form of a Gaussian function which extends down to the targets, a half way between the strongly localized source and the uniform one. It is perhaps obvious that parallel gradient length scales Lk are not as sharp as in the previous case. Shortly, pressure peaks transferred from the stagnation point to the targets are not so pronounced, parallel Mach number is smaller on the average, the intensity of parallel losses $S^n_{\parallel}$ and $S^T_{\parallel}$ is smaller too and the comparison with ESEL does not display so dramatic difference. We can again see a substantial reflection (Fig.14).

In sections 4.1 and 4.2, parallel transport of a blob passing across the flux tube has been analyzed for a simple case when cross-field sources of particles and energy are prescribed as a step function in time. The large turbulent transport seems to be the main source of plasma in the flux tube and processes at the targets (the recycling and ionization representing a source for plasma) become less relevant than in the steadystate analysis. Therefore the form of the cross-field sources is important and the spatial scales of density and temperature variations Lk depend on the parallel profile of these sources and the intensity of their fluctuations. The parallel damping of the density and temperature is stronger for a source localized in a narrow region close to the midplane than for a source that is broader in the parallel direction, as it is shown in Fig.12 and 13. We do not have, however, precise knowledge of the source distribution for the investigated case and it is also difficult to estimate how the parallel profiles of the sources change radially across the SOL. We therefore follow a rough estimate based on experimental results in [19] for the Tore Supra limiter tokamak.

4.3. SIMULATION WITHOUT NEUTRALS

The following figures show results for the same case as above in section 4.1 (Fig.6–12) obtained for a run without neutrals (no ionization within the SOL is present and only cross-field transport is the source of plasma). Without the effect of plasma-neutral interactions, we do not observe two distinct temporal scales and the convection time scale is shorter compared to the previous case as there is no neutral drag (the transient burst at the midplane initiated at t = 0.03s is followed by the maximum target density at t = 0.09s). We observe a supersonic front moving toward the targets (Fig.15) instead of two pronounced density peaks. The heat transport is almost equally shared by the conduction and convection in the initial steady state (Fig.16). Total parallel losses of plasma and

energy calculated at the midplane depends, however, on the source of plasma here, and it appears that they are again stronger than in the ESEL model and the amplitude of $S^n_{\parallel}$ and $S^E_{\parallel}$ ($S^E_{\parallel}$ in Fig.16) is approximately the same as in the run with neutrals (Fig. 11).

4.4. SIMULATION WITH ASYMMETRIC CROSS-FIELD SOURCE

Cross-field sources are prescribed with Gaussian distribution along the field line and localized at the midplane which was represented by the centre of the computational domain, i.e. symmetric situation was considered in the previous sections. However, an asymmetry could be included by moving the particle and power sources (section 4.4), adding a parallel momentum to incoming particles (section 4.5) or a dependence on the toroidal magnetic field (not discussed here).

In figure 17 (steady-state profiles), the asymmetry is induced by shifting the source (midplane) towards one of the targets. While the right target is attached (temperature above 5eV), a detachment occurs at the left target as a result of the dependence of the parallel SOL collisionality on the connection length, see the equation (14). If a transient appears, the asymmetry is associated with later arrival of particles and higher density in front of one of the targets (Fig.18), while the velocities of particles propagating in both directions are equal. The fraction of particle and energy fluxes integrated over the simulated interval 0.5ms on the target which is closer to the source is 84% (for the heat flux) and 61% (for the particle flux).

Figure 19 gives detailed description of particle and energy fluxes arriving at both targets. We can see that the asymmetry is much more pronounced in energy than in the particle flux and results in much higher energy flux to the more exposed target than in the symmetric case. The asymmetry in time caused by different parallel distances is approximately 0.26ms. It is worth noticing that in the dashed profiles of the density or particle flux, we do not observe the initial peak as at the more exposed target or in Fig.10. The structure is dispersed in the parallel direction.

4.5. SIMULATION WITH PARALLEL MOMENTUM SOURCE

The following case is a simulation with symmetric computational domain and particle and energy sources. The asymmetry occurs due to additional parallel momentum carried by incoming particles (a turbulent blob moving in parallel direction). We assume that particles at the midplane have a non zero parallel velocity prescribed toM = 0.5 (typical maximum value we could expect in the SOL). The steady-state solution in Fig.20 does not display a strong asymmetry (again its the ionization of recycled neutrals at the targets which is the main source of plasma and determines the steady-state solution in comparison to less important cross-field sources concentrated around the midplane). Snapshots in Fig. 21 show clearly the momentum source (see the red positive peak of the plasma velocity in the centre associated with the incoming transient burst). Particles propagate to both directions with different velocities, the advection to the right target is stronger and we observe higher density peak (see the green peaks of the density). Fig.22 shows the plasma density along the flux tube in time. The fraction of particle and energy fluxes integrated over the simulated interval

on the preferential target is 58% (for the heat flux) and 54% (for the particle flux).

Fluxes at the targets are plotted in Fig.23. A comparison with previous results in sections 4.1 and 4.4 shows differences between two asymmetric cases, one induced by different parallel distances on both side, the second by initial convective parallel velocity to one target. The time shift of fluxes between both targets in Fig.23 is not significant (time scales are determined by the collisionality regime of the SOL) and the level of asymmetry of peak fluxes is comparable for particles and energy. Table 1 summarizes particles and energy loads on the targets for three simulated cases, case 1 – the reference symmetric case (section 4.1), case 2 – the turbulent blob entering the domain closer to one of the targets (section 4.4) and case 3 – the moving blob (section 4.5).

4.6. PARALLEL TRANSPORT OF TURBULENT STRUCTURES FOR JET PARAMETERS

Before introducing a new parallel model in the ESEL code, it is useful to investigate the response of SOLF1D to a fluctuating source prescribed by the cross-field turbulent dynamics as modelled in ESEL. If we directly use values of S^n_{EXT} and S^E_{EXT} from Fig.5 that were calculated from ESEL using the approximative model for the parallel terms, we encounter certain problems, namely we can not avoid negative values of the density and temperature due to the fact that the parallel damping in SOLF1D is stronger than in ESEL, which was demonstrated in the previous section. To overcome this inconsistency, we have adapted the code to fluctuations of the density and temperature by using n_e and T_e at the midplane as the input instead of S^n_{EXT} and S^E_{EXT} and the sources are adjusted to obtain the desired density and temperature. In this setup, we can calculate the response to fluctuations in fully time-dependent way and study the effect of turbulent dynamics on the parallel transport. Fig.24 and 25 show results of such time-dependent run. We used ESEL data for the JET run in [9] ($n_{sep} \approx 1 \times 10^{19}\,\mathrm{m}^{-3}$, $T_{sep} \approx 40\mathrm{eV}$, $L_c = 25\mathrm{m}$). The density and temperature at the midplane in SOLF1D copy the ESEL values and the initial condition was obtained as a steady-state for the average density and temperature.

In figure 24, parallel losses in SOLF1D are compared with losses which ESEL would calculate. Results of SOLF1D again show the complexity of the parallel transport compared to the simple predictions (10) and (11) and point out that the parallel damping in the form of loss terms (10) and (11) is not accurate enough. Loss terms are linked with three-dimensional dynamics which excludes their parametrization using the simple (0D) model. The intensity of the parallel losses is stronger and negative values appear as well. We can see that the difference between ESEL and SOLF1D is more significant for the parallel density loss time τ_n than for the electron cooling time τ_T. Let us mention that, while certain success has been achieved in simulating TCV plasma when constant parallel loss times were considered [7], the simulation of the JET SOL in [9, 25] based on loss factors (10) and (11) (the result is shown in Fig.24 on the right) indicate that the parallel transport model in ESEL assuming free streaming with ion sound speed is insufficient. Clearly, the parallel damping of the density should be stronger to match the experimental profile and, based on the presented results, better agreement with experiment is anticipated after improving the ESEL

model or coupling ESEL and SOLF1D. It is worth mentioning that beside the radial density profile, which is broader in simulation than in experiment, ESEL predicts higher temperature fluctuation level compared with the measured one.

Note that negative values of the loss terms $S^n_{\parallel}$ and $S^T_{\parallel}$ are omitted in the ESEL parallel model (the loss terms scale with the density and temperature), but they are in principle possible (Fig.24). The transit of a blob across the flux tube in terms of cross-field sources can be illustrated as a sharp source of plasma followed by a negative tail when the blob is leaving the flux tube. The opposite parallel gradients of the density and temperature may occur at the midplane and the plasma and the heat from the SOL tend to refill the remaining hole. Stronger negative peaks are observed for the electron cooling term $S^T_{\parallel}$, again due to the diffusive character of the heat transport. Also in the previous section, we could find negative $S^n_{\parallel}$ at the midplane when a fraction of plasma from the ionization zones appeared back at the midplane (the reflection in Fig.9 and 14). These effects are missing in ESEL.

Figure 25 shows fluctuating density and temperature at the midplane (the ESEL result and the input for SOLF1D) and the corresponding response at the target. SOLF1D provides a tool for investigating the difference between steady-state description of parallel transport and time-dependent description taking into account plasma fluctuations. The simulation indicate that the time average values of plasma parameters along the SOL differ from the initial stationary state which was obtained for a constant midplane density and temperature calculated as the average over the investigated time interval. This is due to the fact that parallel transport parameters as transport coefficients and collision rates are in general nonlinear functions of the density and temperature. It is the subject of a separate paper [24] where longer time series of ESEL output are used to obtain reasonable statistics. In [24], parallel transport parameters which are important in the SOL dynamics are compared in a steady state and timedependent case and the impact of fluctuations is estimated with regards to the steadystate description widely used in the present-day edge fluid codes such as SOLPS or

CONCLUSIONS

Plasma transport in the SOL between targets has been studied by means of the onedimensional fluid code SOLF1D with the aims to provide insight into parallel SOL dynamics and to carry out analysis leading to improved calculation of losses of plasma and heat along the magnetic field in the turbulence code ESEL. The parallel transport in ESEL appears in the form of loss terms. A comparison of these terms with SOLF1D solutions has been done both for a steady-state SOL (following the assumption of the parallel transport model in ESEL and for the purpose to test the approximative model itself under different collisionality regimes) and a turbulent SOL (time-dependent modelling of parallel transport processes taking into account fluctuations which we observe as a consequence of edge turbulence).

It was shown that in steady state, the tokamak operational regime and its collisionality (we distinguish between the simple and complex SOL) determine the stationary solution along the SOL

and that the processes at the target of neutral recycling and ionization are important factors for constituting gradients of plasma parameters in the parallel direction, which drives plasma transport along the SOL and determines the strength of parallel losses.

Further, we focused on a transient situation and we simulated a blob event and its parallel damping. We have found two distinct time scales of transport processes, corresponding to electron thermal and ion sound speed. It can be deduced from the results that for a precise calculation of the parallel loss terms, dynamics should not be neglected and a steady-state description is not adequate. The ESEL model based on (10) and (11) underestimates parallel losses, especially for particles, and using SOLF1D to replace the simple approximations in ESEL would improve the ESEL physics. The presented results are also promising in the sense of a comparison of ESEL with experiments.

The key parameters responsible for establishing the parallel gradient scale $L_{\|}$ are radial sources of particles and energy from the outboard midplane, displaying large fluctuations due to turbulence, and their temporal and spatial distribution. Parallel Mach number increases compared to steady-state values and the processes at the target of recycling and ionization are not as relevant as in the steady-state description of the SOL. Further, we have found evidence that the convection-based transport of particles establishes $L^{n}_{\|}$ that is distinct from $L^{T}_{\|}$ for the temperature driven by the diffusiondominated transport and we remark that the simple ESEL model uses $L_{\|} = L_c$ both for the density and temperature.

Additional effects have been analyzed in the transient case, (i) the effect of neutrals on the parallel time scale and parallel Mach number, (ii) the effect of asymmetry imposed by a cross-field source which is closer to one of the targets (justified by observed preferential outflow at the outboard side due to ballooning), (iii) asymmetry assuming a certain initial parallel momentum of particles in this source (initial rotation of plasma).

ACKNOWLEDGMENTS

The authors acknowledge helpful discussions with colleagues during the EFDA-JET edge modelling months, specifically D. Coster, F. Subba, A. Chankin, D. Tskhakaya and S. Wiesen. This work was supported by the Associations Risø, IPP.CR and EURATOM and carried out within the framework of the European Fusion Developlment Agreement. The views and opinions expressed herein do not necessarily reflect those of the European Commission. The main author acknowledges partial support of Czech Science Foundation, Grant No. 205/10/2055, and MSMT CR, Grant No. 7G09042. The CCFE authors were funded by the RCUK Energy Programme under grant EP/G003955.

REFERENCES

[1]. Zweben S.J. et al 2007 Plasma Physics and Controlled Fusion **49** S1
[2]. Boedo J.A. 2009 Journal of Nuclear Materials **390-391** 29
[3]. Krasheninnikov S.I. et al 2008 Journal of Plasma Physics **74** 679
[4]. Xu G.S. et al 2009 Nuclear Fusion **49** 092002

[5]. Falchetto G.L. et al 2008 Plasma Physics and Controlled Fusion **50** 124015
[6]. Garcia O.E. et al 2005 Physics of Plasmas **12** 062309
[7]. Garcia O.E. et al 2006 Plasma Physics and Controlled Fusion **48** L1
[8]. Braginskii S.I. 1965 Review of Plasma Physics **1** 205
[9]. Fundamenski W. et al 2007 Nuclear Fusion **47** 417
[10]. Fundamenski W. 2005 Plasma Physics and Controlled Fusion **47** R163
[11]. Tskhakaya D. et al 2009 Journal of Nuclear Materials **390-391** 335
[12]. Zagórski R. 1996 Journal of Technical Physics **37** 7
[13]. Huba J.D. NRL plasma formulary (Naval Research Laboratory, Washington)
[14]. Karniadakis G.E. et al 1991 Journal of Computational Physics **97** 414
[15]. Havlíčková E. 2009 PhD thesis (Charles University, Prague)
[16]. Garcia O.E. et al 2007 Nuclear Fusion **47** 677
[17]. Stangeby P.C. 2000 Plasma Physics and Controlled Fusion **42** B271 Parallel transport in the SOL 26
[18]. Stangeby P.C. 2000 The plasma boundary of magnetic fusion devices (Bristol: IOP Publishing)
[19]. Gunn J.P. et al 2007 Journal of Nuclear Materials **363-365** 484
[20]. Schneider R. et al 2006 Contribution to Plasma Physics **46** 3
[21]. Taroni A. et al 1992 Contribution to Plasma Physics **32** 438
[22]. Simonini R. et al 1994 Contribution to Plasma Physics **34** 368
[23]. Coster D.P. et al 2005 Journal of Nuclear Materials **337-339** 366
[24]. Havlíčková E. et al PSI conference 2010 (to be published in Journal of Nuclear Materials)
[25]. Naulin V. et al 2006 Proceedings 21st IAEA Fusion Energy Conference TH/P6-22

	Case 1	Case 2	Case 3
$\Gamma^{right}_{peak} / \Gamma^{left}_{peak}$	1.00	2.14	1.84
$\Gamma^{right}_{integral} / \Gamma^{left}_{integral}$	1.00	1.56	1.17
$Q^{right}_{e,peak} / Q^{left}_{e,peak}$	1.00	8.55	2.48
$Q^{right}_{e,integral} / Q^{left}_{e,integral}$	1.00	5.25	1.33
$Q^{right}_{i,peak} / Q^{left}_{i,peak}$	1.00	12.00	2.99
$Q^{right}_{i,integral} / Q^{left}_{i,integral}$	1.00	5.25	1.44

Table 1: Fractions of particle flux $\Gamma = \Gamma_i = \Gamma_e$, electron heat flux Q_e and ion heat flux Q_i to the targets for three investigated cases (case 1 – symmetric case, case 2 – blob closer to the right target, case 3 – blob moving towards the right target). Two numbers for each flux are the ratio of the peak value at the right and left target and the ratio of time-integrated flux to the right and left target.

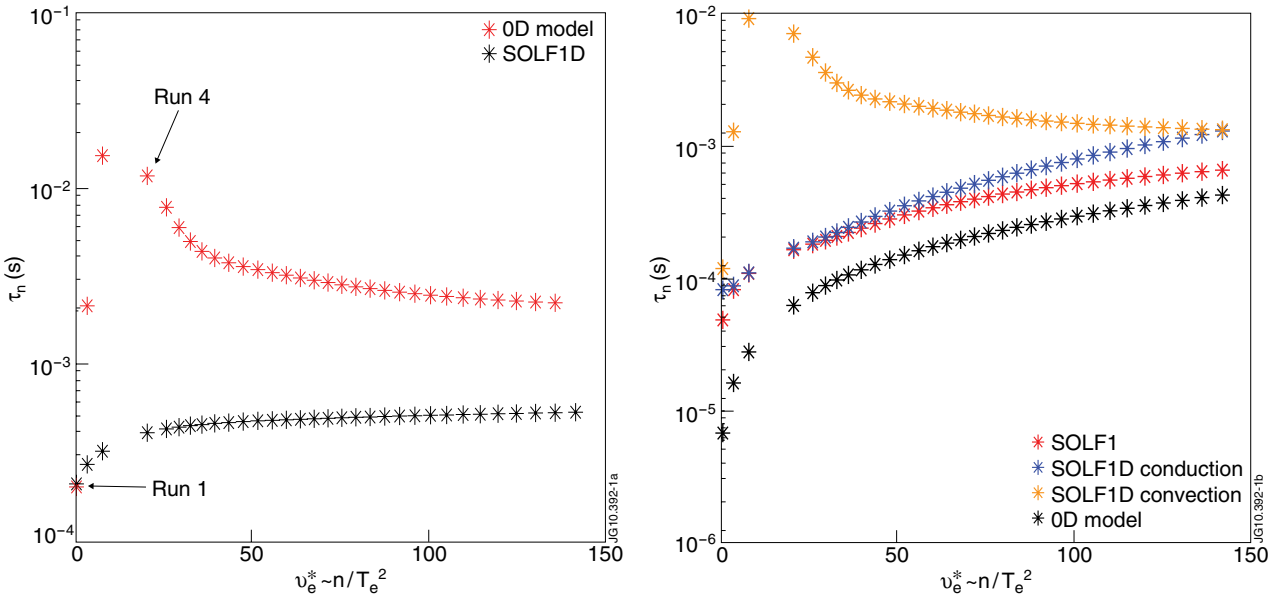

Figure 1: The parallel particle density and energy loss times τ_n and τ_E as functions of the electron collisionality ν_e^* for steady-state solutions. A comparison of SOLF1D (red) and the 0D model used in the ESEL code (black).

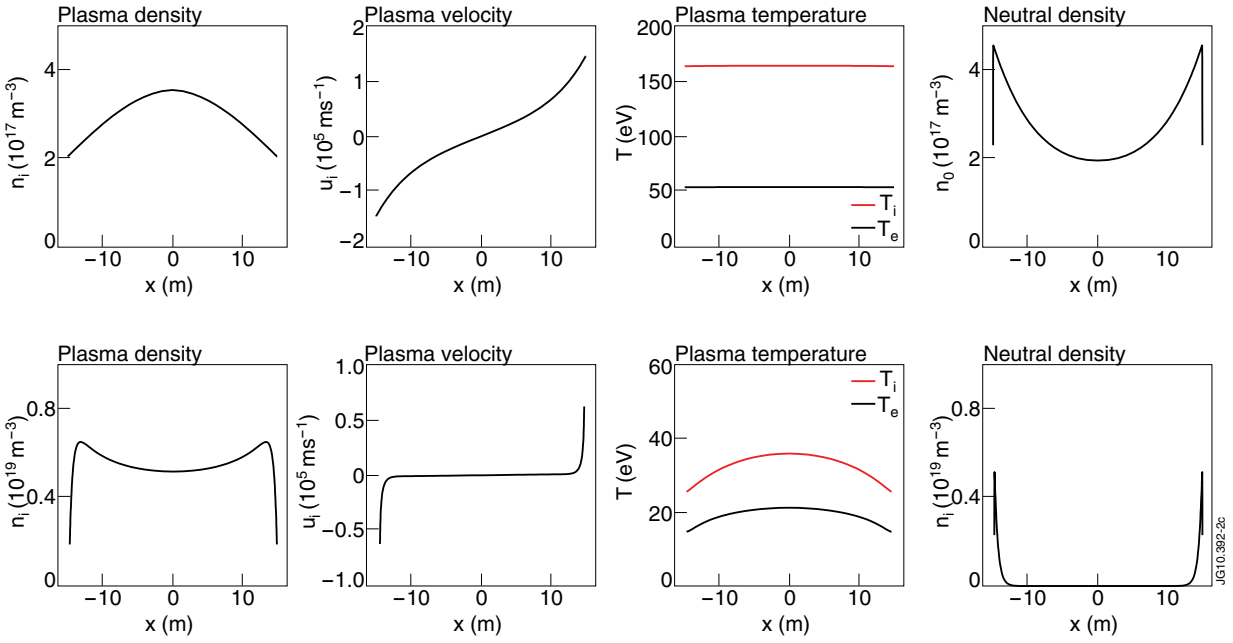

Figure 2. Parallel profiles of plasma parameters. A transition from the simple SOL (the top row – run 1 from Fig.1) to the complex SOL (the bottom row – run 4 from Fig.1).

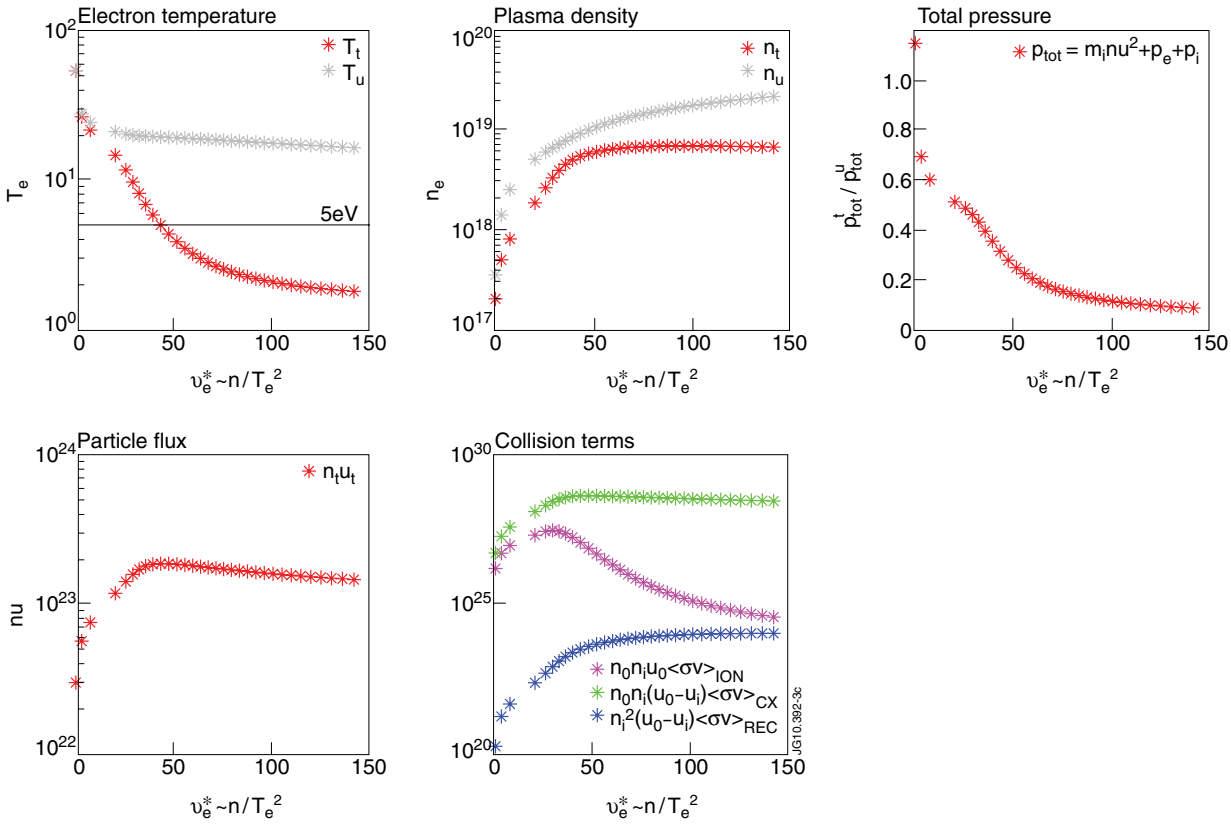

Figure 3: Upstream (u) and target (t) plasma parameters and contributions of ionization, charge exchange and recombination in the momentum balance at the target in different collisionality regimes.

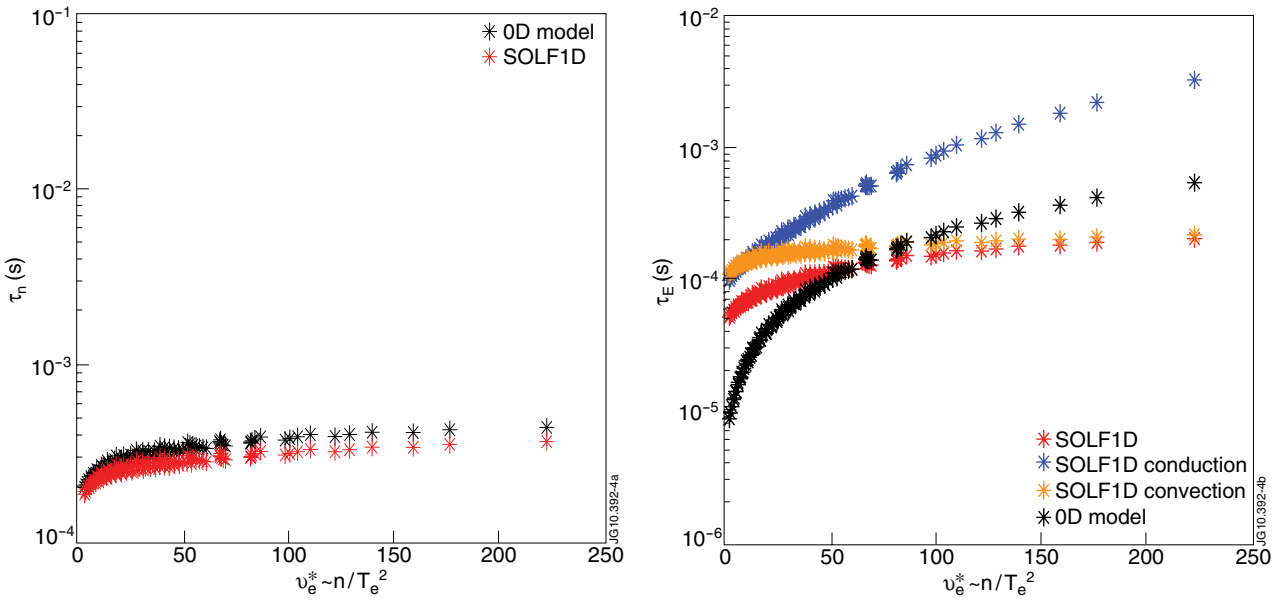

Figure 4: The parallel particle density and energy loss times τ_n and τ_E as functions of the electron collisionality ν_e^* for steady-state solutions. A scan without the effect of plasma-neutral collisions.

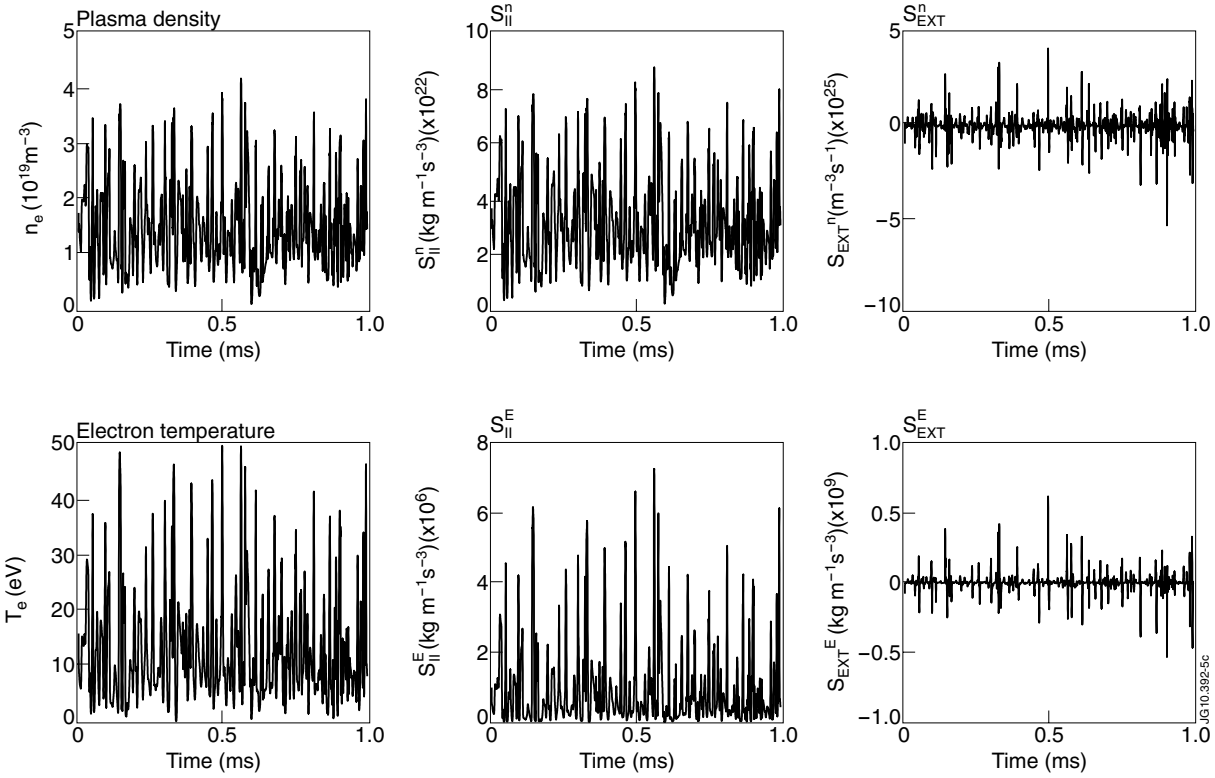

Figure 5: Data from ESEL used as the input for SOLF1D – the plasma density n_e, the electron temperature T_e, the total parallel particle and energy losses $S_{||}^{n}$ and $S_{||}^{E}$ and the corresponding cross-field terms S^{n}_{EXT} and S^{E}_{EXT}.

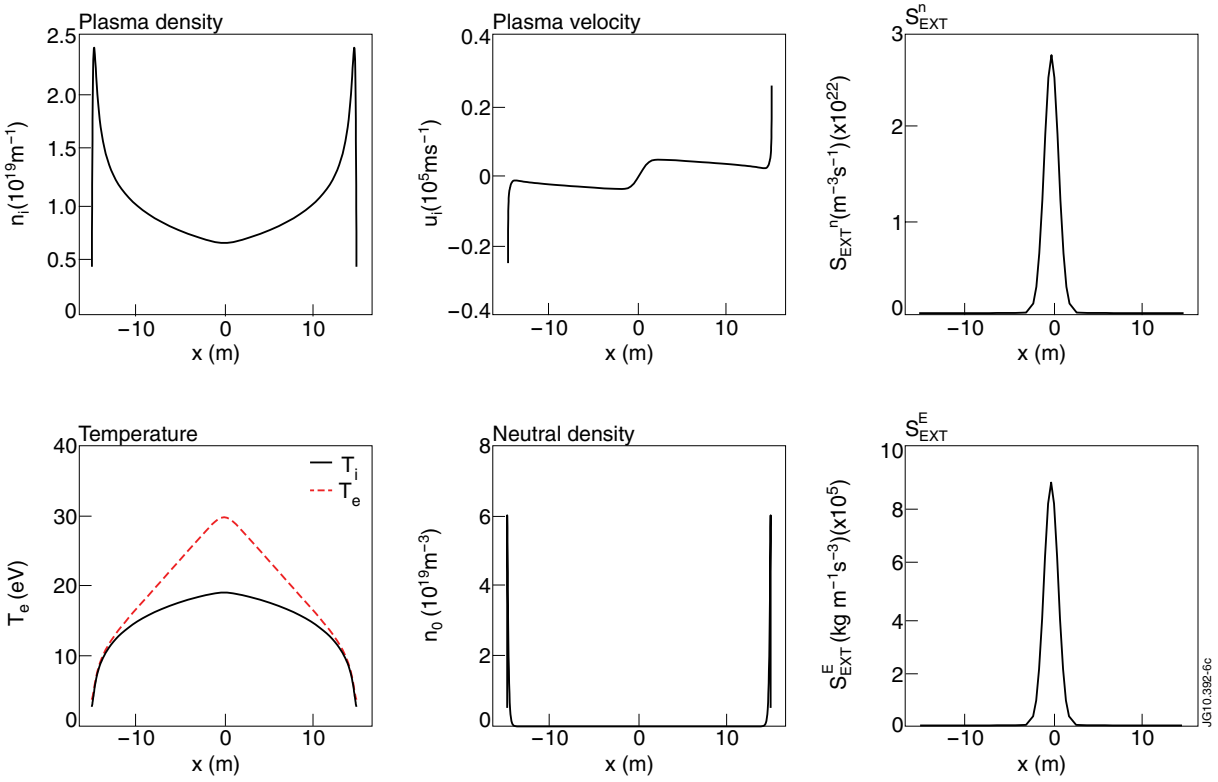

Figure 6: Steady-state parallel profiles of plasma parameters and cross-field sources.

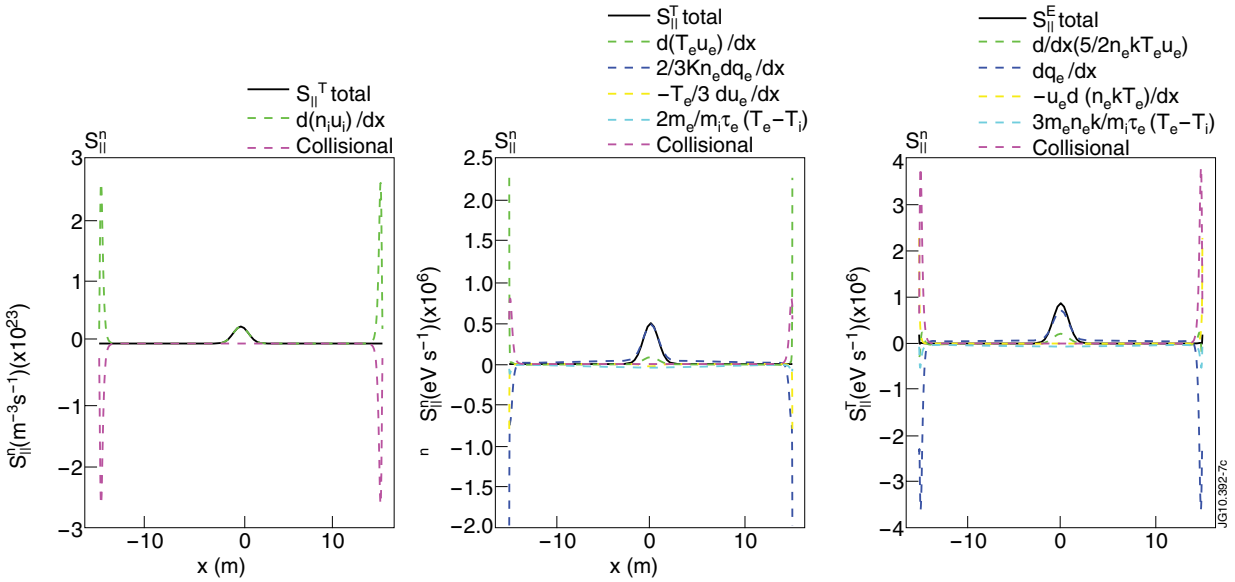

Figure 7: The total parallel particle, temperature and energy losses $S_{\parallel}^{\ n}$, $S_{\parallel}^{\ T}$ and $S_{\parallel}^{\ E}$ and contributions of all individual terms in the steady-state solution.

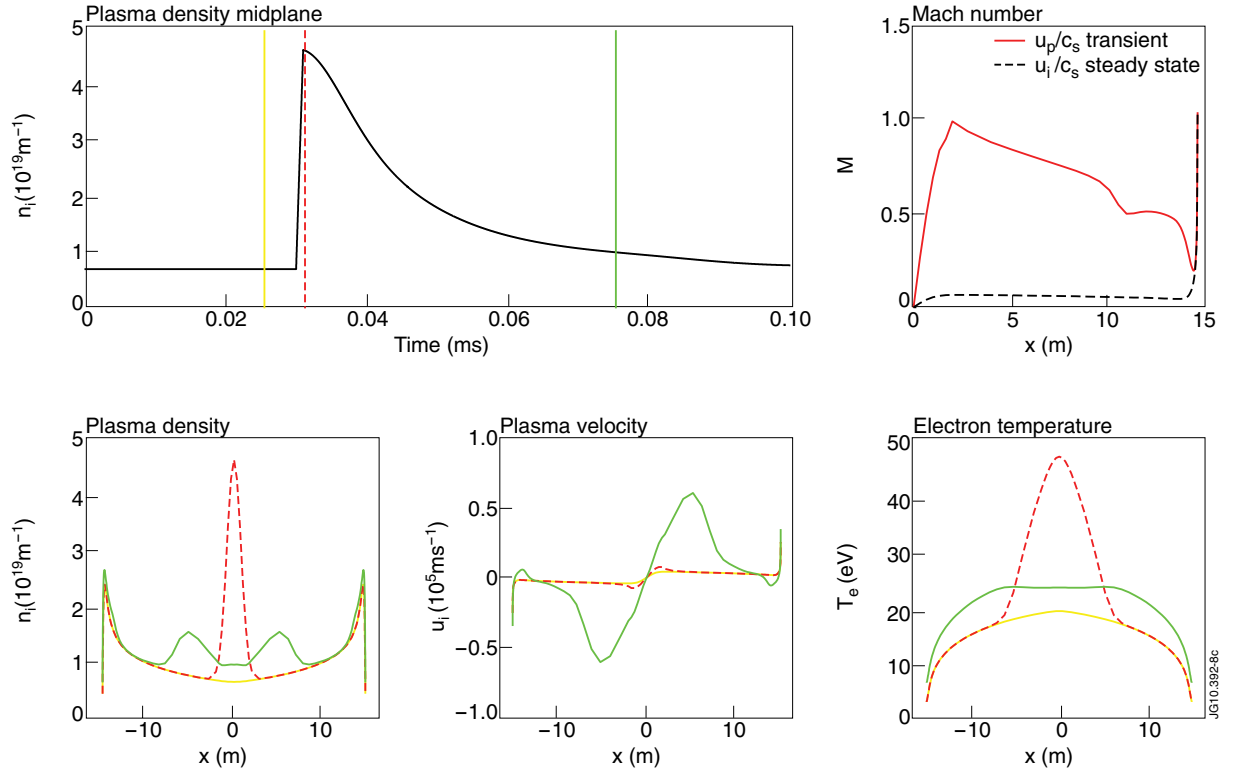

Figure 8: Parallel profiles of the plasma density n_i, the plasma velocity u_i and the electron temperature T_e at three selected moments (bottom) and the parallel velocity (top right) of the density peak u_p (see the green peaks of the density) at each passed parallel position x calculated as the plasma velocity u_i at t_{max} when the density at x reaches the maximum. The ion sound speed c_s is calculated at each position x at t_{max}. The parallel Mach number is compared to the steady-state value.

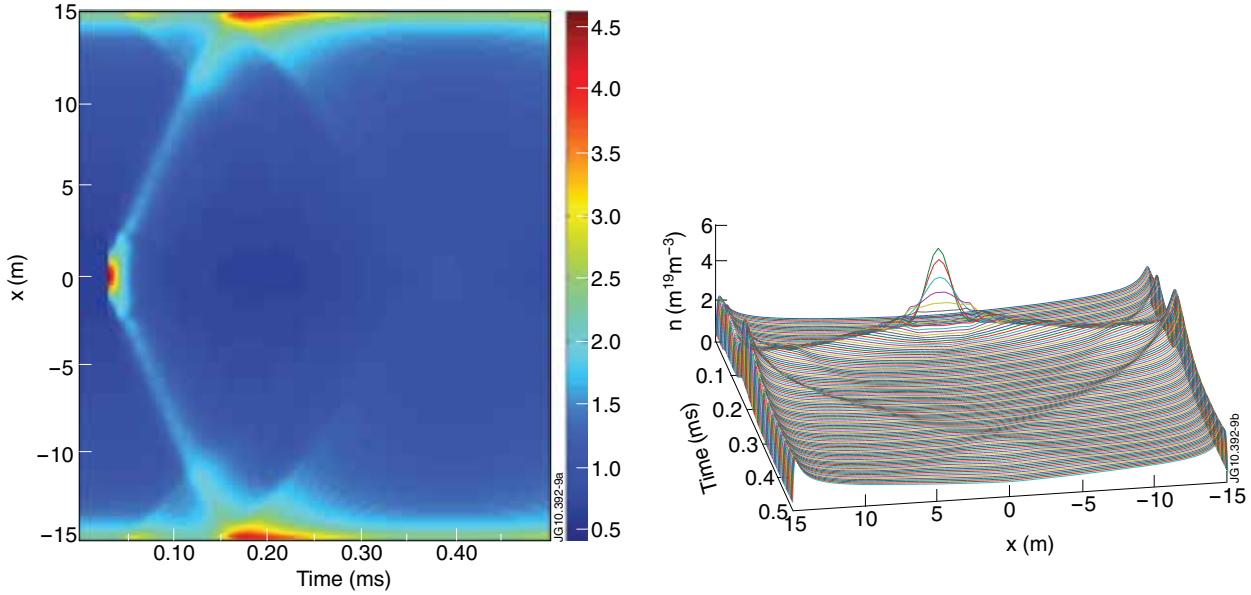

Figure 9. The plasma density n_i (10^{19} m^{-3}) during a transient event and propagation of particles to the targets.

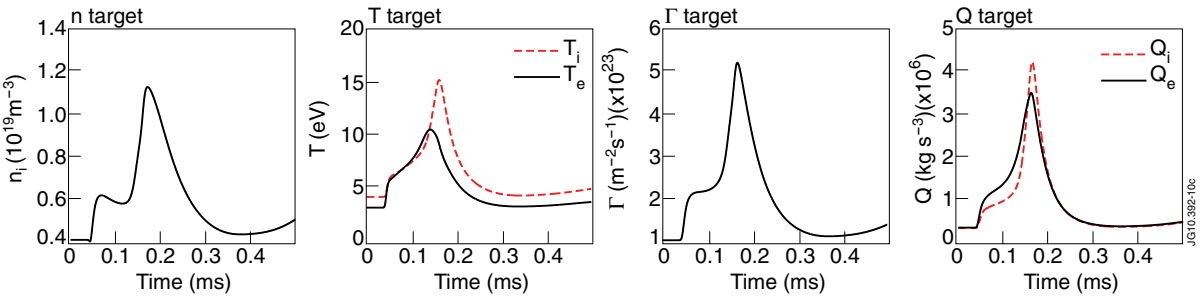

Figure 10: Plasma density, temperature, particle flux and energy flux at the target during a transient burst.

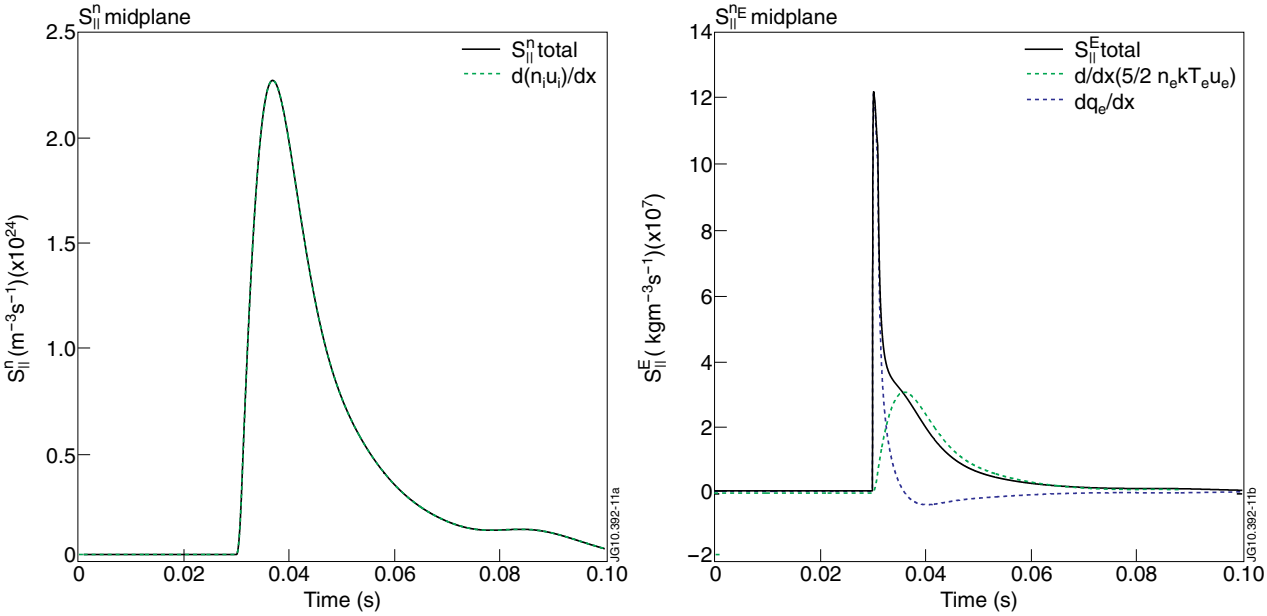

Figure 11: The total parallel density and energy losses $S^{n}_{||}$ and $S^{E}_{||}$ and conduction and convection contributions to the energy transport for a blob which occurred at the midplane.

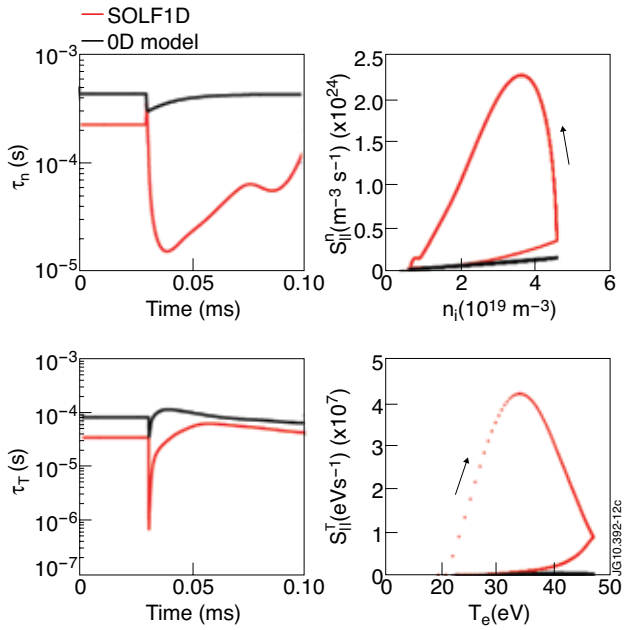

Figure 12: The parallel particle density loss time n and the electron cooling time τ_n (left) and the total parallel losses $S_{||}^{\ n}$ and $S_{||}^{\ T}$ as functions of the density ni and temperature T_e (right).

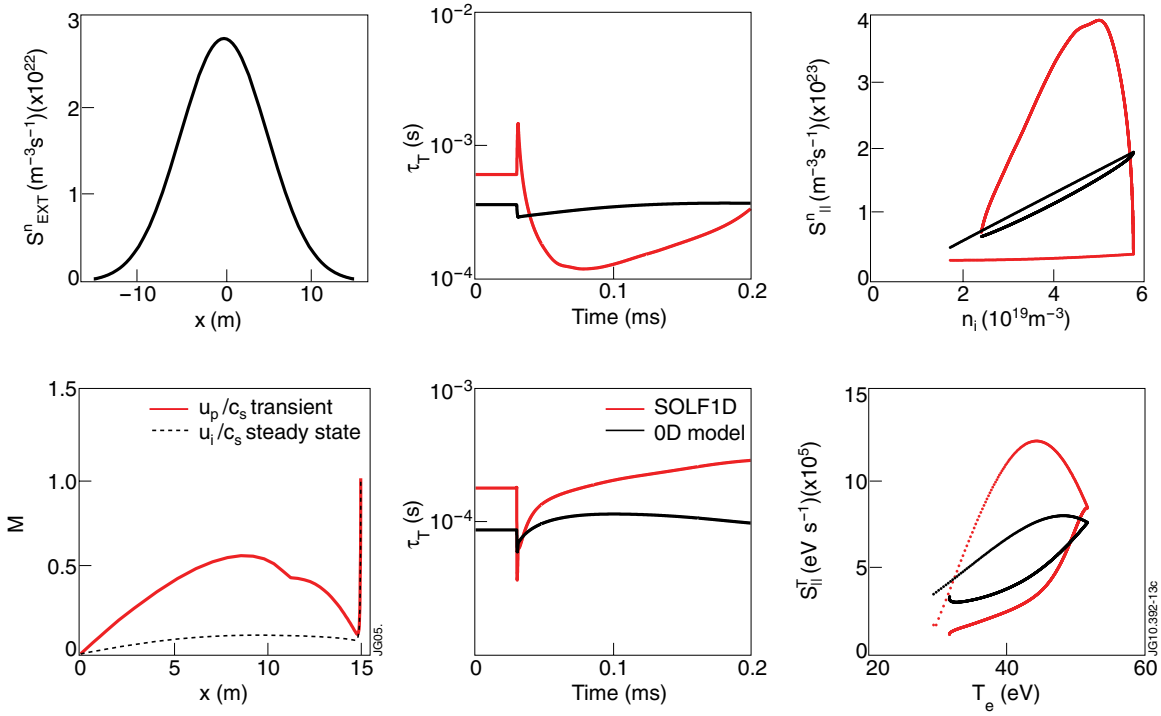

Figure 13. The density source S^n_{EXT}, the parallel Mach number M of the perturbation transit, the parallel loss times τ_n, τ_T and the total parallel losses $S_{||}^{\ n}$, $S_{||}^{\ T}$.

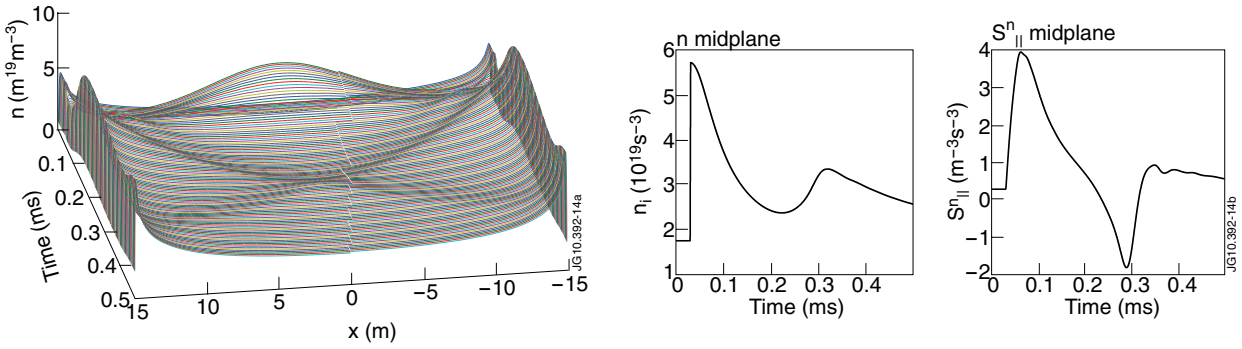

Figure 14: The plasma density ni and the parallel loss term of the density $S_{||}^{n}$. at the midplane.

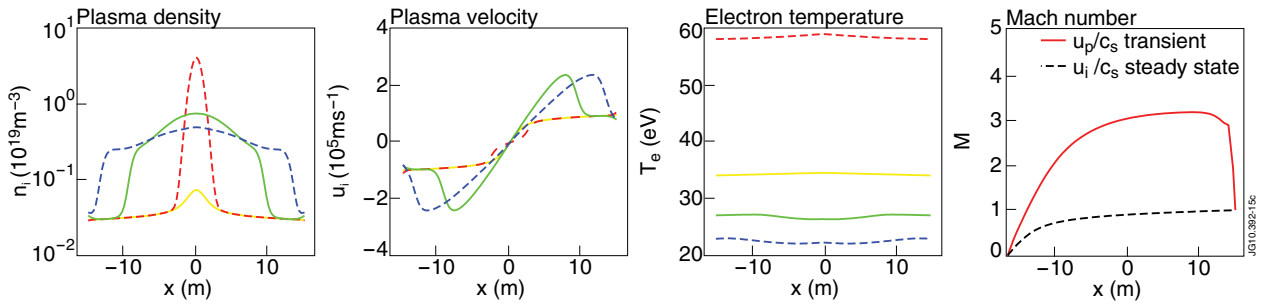

Figure 15: Parallel profiles of the plasma density n_i, the plasma velocity ui and the electron temperature T_e at t = 0.025ms (yellow), t = 0.031ms (red), t = 0.06ms (green) and t = 0.075ms (blue). The velocity of propagation of the supersonic front u_p (right) normalized by the local ion sound speed c_s and compared to the parallel Mach number in steady state.

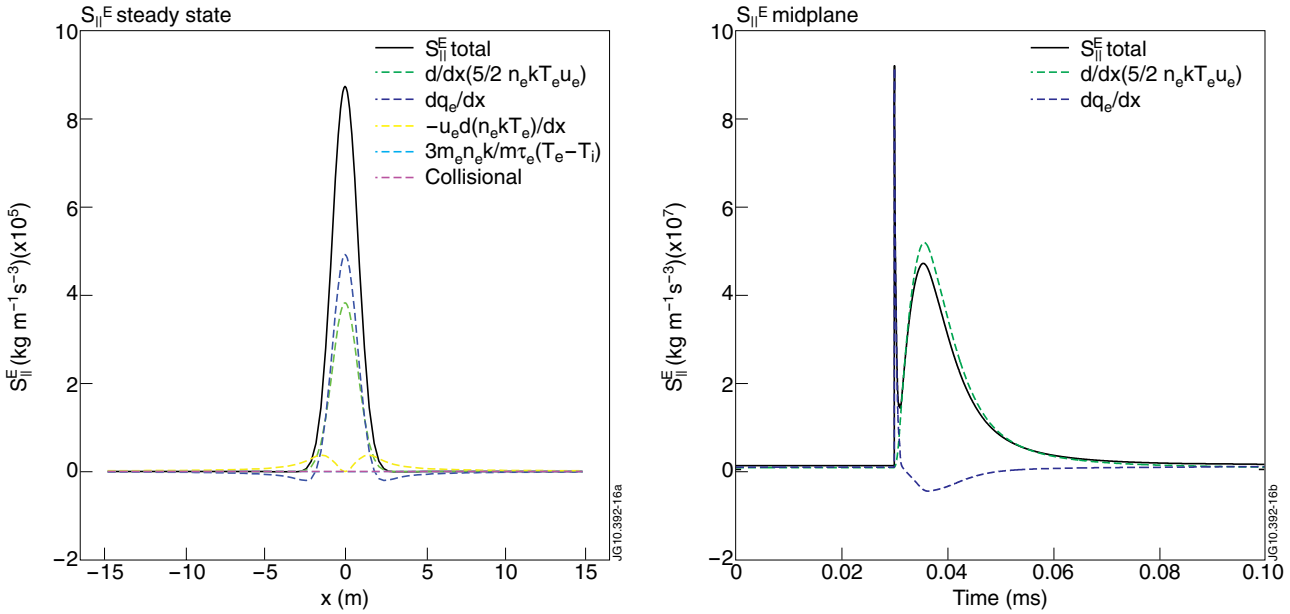

Figure 16: The total energy losses $S_{||}^{n}$ and conduction (blue) and convection (green) contributions in a steady state (left) and during a transient event (right) when interactions with neutrals are absent.

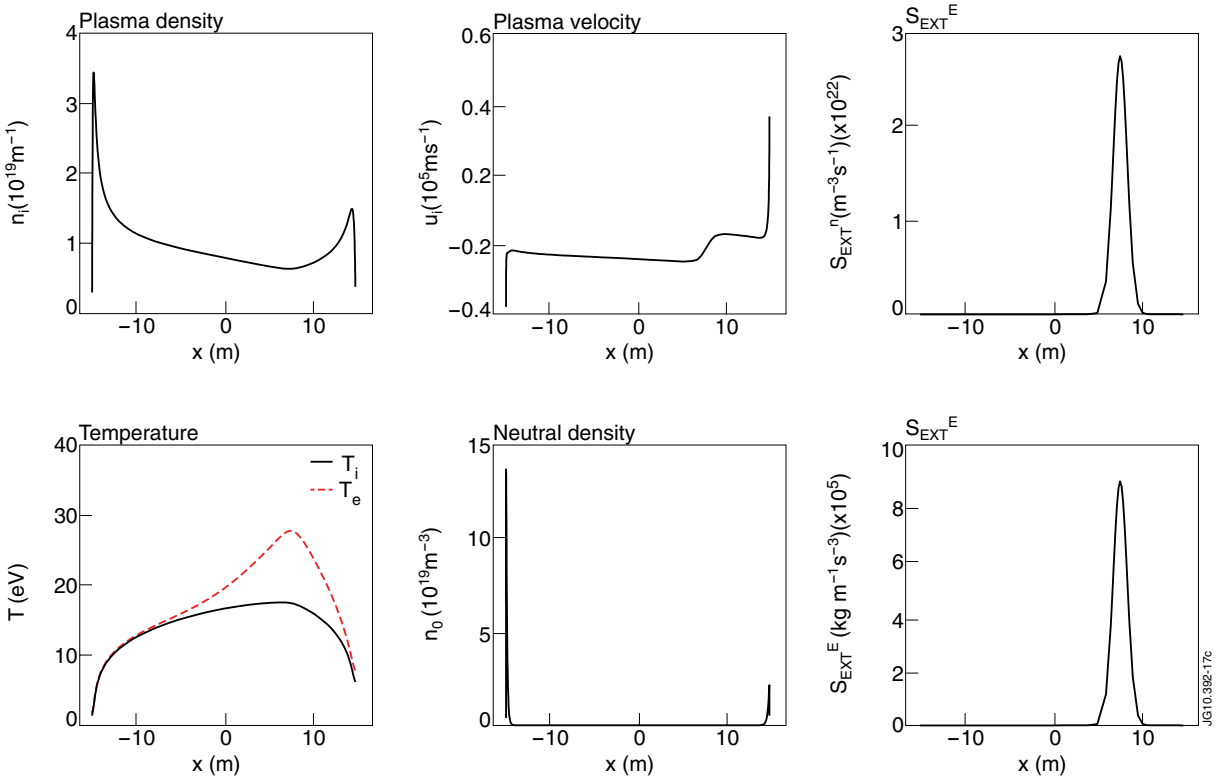

Figure 17: Steady-state parallel profiles of plasma parameters and cross-field sources.

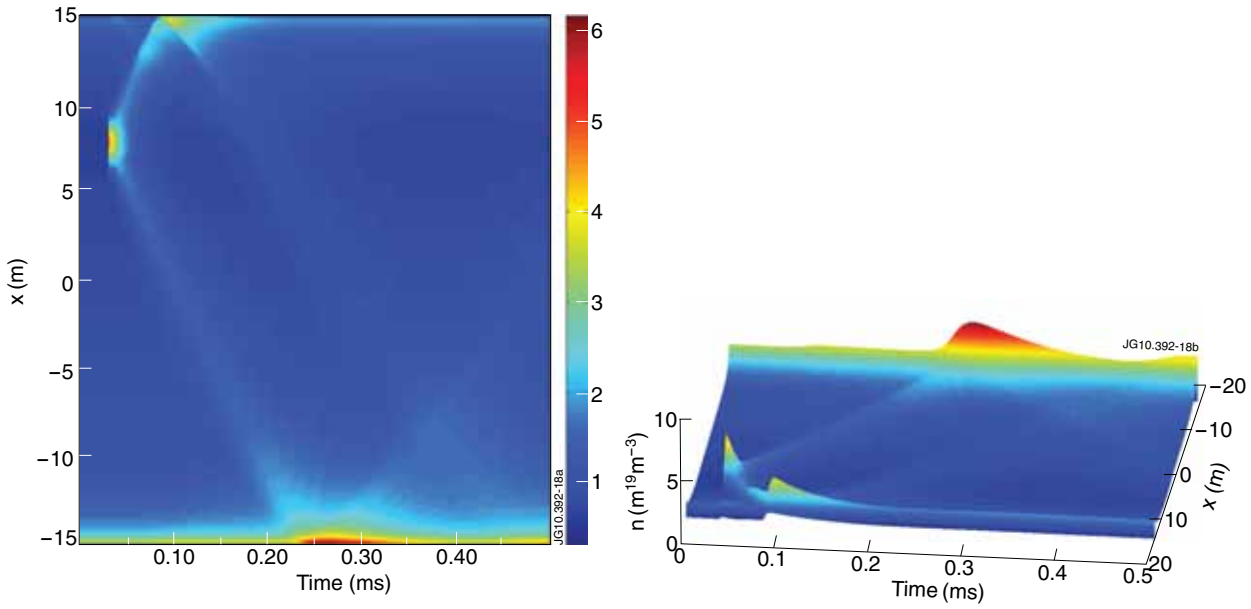

Figure 18:The plasma density $n_i(10^{19}\,m^{-3})$ during a transient event. The asymmetry is induced by prescribed particle and energy sources appearing closer to one target.

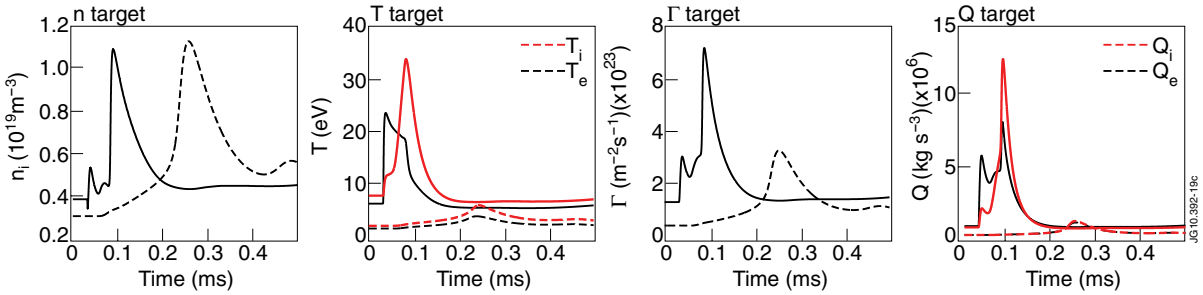

Figure 19: Plasma density, temperature, particle flux and energy flux at the left (dashed line) and right (solid line) target during a transient burst.

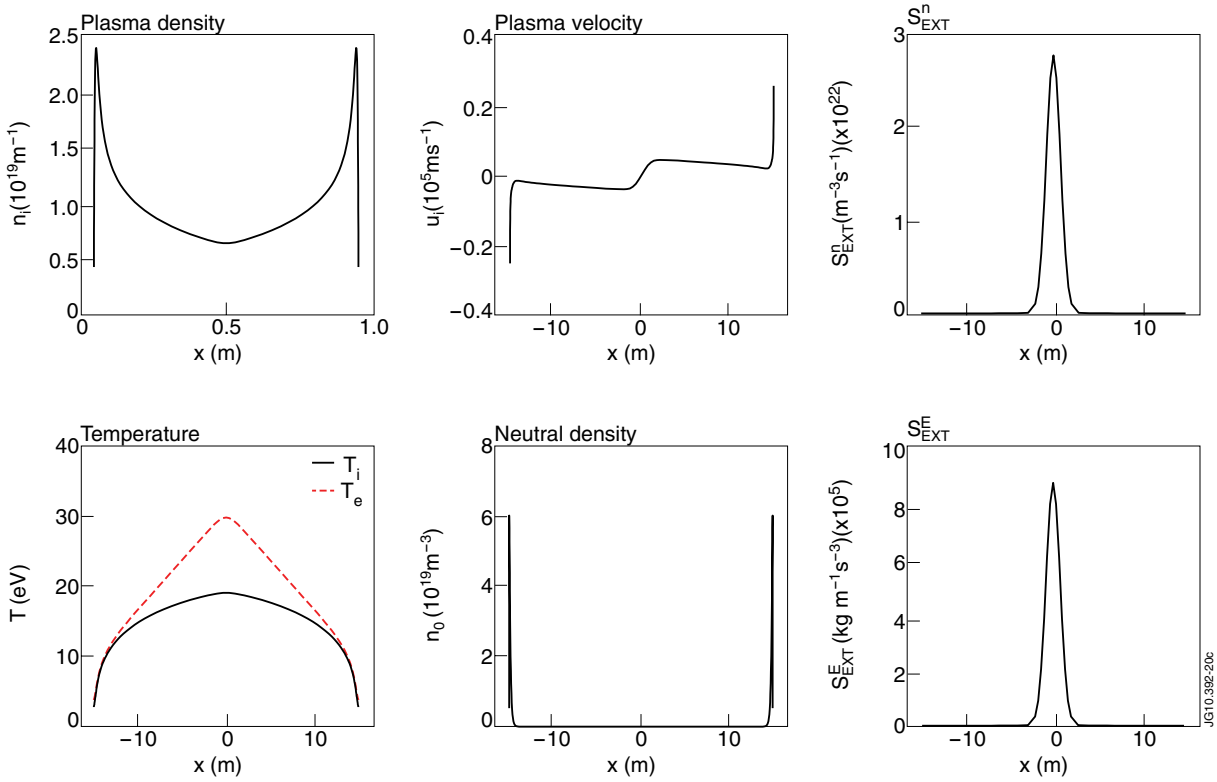

Figure 20: Steady-state parallel profiles of plasma parameters and cross-field sources.

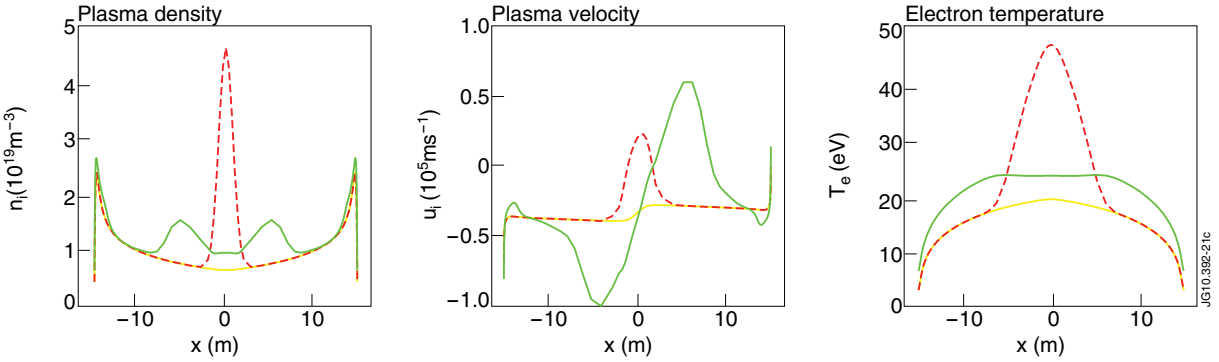

Figure 21. Parallel profiles of the plasma density ni, the plasma velocity ui and the electron temperature T_e at t = 0.025ms (yellow), t = 0.031ms (red) and t = 0.075ms (green).

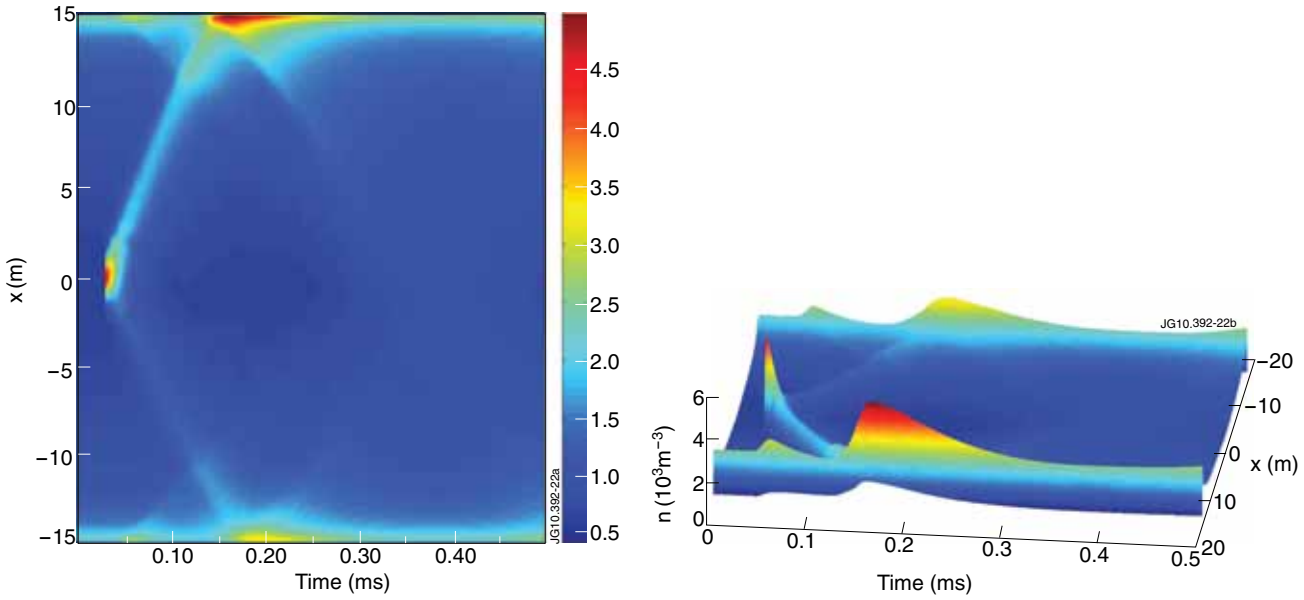

Figure 22: The plasma density $n_i (10^{19}\, m^{-3})$ during a transient event. The asymmetry is induced by additional parallel momentum source.

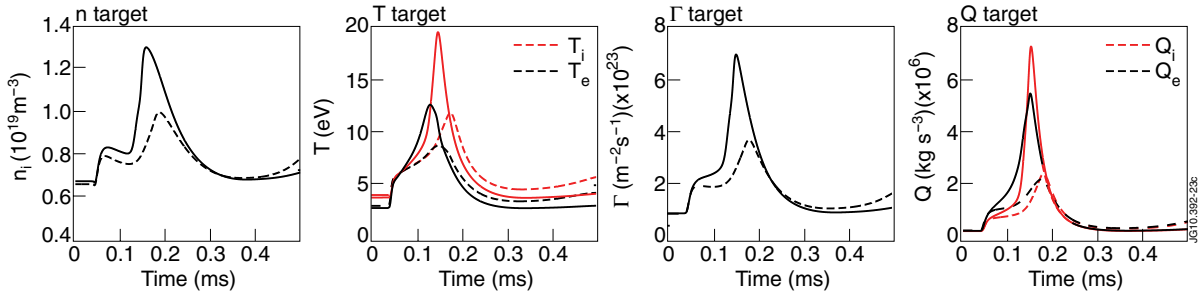

Figure 23: Plasma density, temperature, particle flux and energy flux at the left (dashed line) and right (solid line) target during a transient burst.

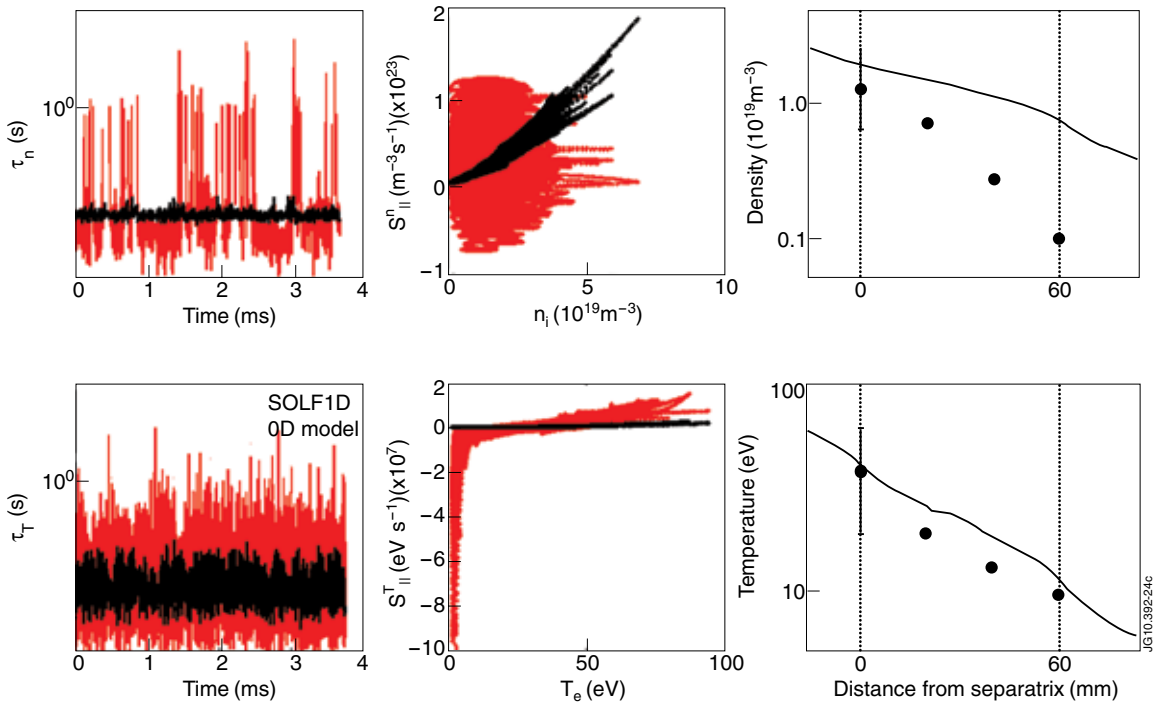

Figure 24: The parallel particle density loss time τ_n, the electron cooling time τ_T, the total parallel losses $S_{||}^{n}$ and $S_{||}^{T}$ as functions of the density ni and temperature Te. On the right (reprinted from [9]), radial profiles for an Ohmic JET discharge calculated in ESEL, a comparison of simulation (solid line) and experiment.

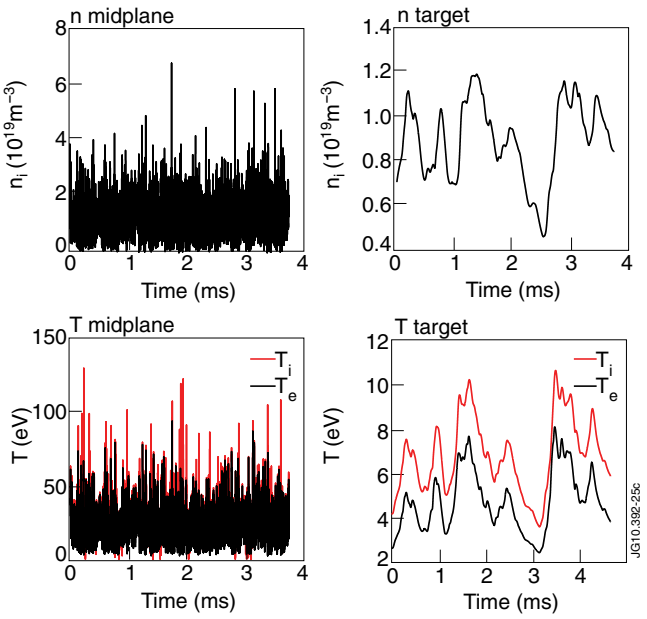

Figure 25: Temporal profiles of the plasma density n_i and temperature T_e and T_i at the midplane and target.